Computers and Concrete, Vol. 8, No. 1 (2011) 97-110
DOI: http://dx.doi.org/10.12989/cac.2011.8.1.097

Application of computational technologies to R/C structural analysis

Takashi Hara*

Department of Civil Engineering and Architecture, Tokuyama College of Technology, Gakuendai, Shunan 745-8585, Japan

(Received September 24, 2009, Accepted March 10, 2010)

Abstract. In this paper, FEM procedure is applied to the static and dynamic analyses of R/C structures. Simple R/C shell structure is solved by using FEM procedures and the experimental evaluations are performed to represent the applicability of FEM procedure to R/C structures. Also, R/C columns are analyzed numerically and experimentally. On the basis of these results, FEM procedures are applied to the R/C cooling tower structures assembled by huge R/C shell structure and a lot of discrete R/C columns. In this analysis, the parallel computing procedures are introduced into these analyses to reduce the computational effort. The dynamic performances of R/C cooling tower are also solved by the application of parallel computations as well. From the numerical analyses, the conventional FEM procedures combined with computational technologies enables us to design the huge R/C structures statically and dynamically.

Keywords: FEM analysis; R/C shell; parallel computing; computational mechanics.

1. Introduction

Several FEM procedures have been proposed and applied to simulate many kinds of reinforced concrete (R/C) structures (Hinton *et al.* 1984, 1986 and Hara *et al.* 1996, 2003). Although there are much unresolved problems, such as the constitutional representations of materials or discrete phenomena after cracking of concrete, these schemes are useful tools to design R/C structures based on the comparisons between numerical and experimental results. On the other hand, due to the progress of computational technologies, additional computational schemes have been introduced into the FEM analysis. A grid computing is useful to design the structure parametrically based on the optimal designing concepts. A parallel computation is also applied to solve the huge structure or the problems for the local behavior within huge complex structures (Adeli *et al.* 1999).

Such computational technologies have been applied to the analysis of R/C structures recently. Several numerical results are compared with the experimental results and the applicability of FEM scheme to particular R/C structures has been verified. However, the evaluation of both numerical and experimental results concerning R/C shell structures has been still required. Especially, the safety evaluation of huge industrial R/C structures under the static and the dynamic loading are the important problems. Due to the solutions of the environmental problems concerning the balances between the reduction of carbon dioxide and the growth of global economy, the huge R/C cooling tower has been rebuilt (Busch *et al.* 2002) and the R/C solar chimney was proposed (Harte *et al.*

* Professor, Dr. of Eng., E-mail: t-hara@tokuyama.ac.jp

2009) recently.

In this paper, FEM is applied to the analysis of several R/C structures composing a complex huge R/C structure. Firstly, simple R/C shell structures are solved by use of FEM based on the degenerate shell discretization. Experimental evaluations are performed under the same loading and supporting conditions so as to compare the both numerical and experimental results. Secondary, R/C columns are also analyzed numerically and experimentally. In numerical analysis, the solid element discretization is applied. Both results show in good agreement. Finally, on the basis of these result mentioned above, FEM is applied to solve the huge R/C cooling tower structure problems. In this analysis, parallel computing procedures are introduced into the analysis in order to reduce the computational effort. An R/C cooling tower has a huge R/C shell which is supported by discrete R/C columns. The dynamic performances of R/C cooling tower are also computed by the application of parallel computations.

2. Thin R/C shell under concentrated load

Thin R/C cylindrical shell structure supported on meridional edges under concentrated load (see Figs. 1 and 2) is analyzed numerically and experimentally to evaluate the applicability of the degenerate shell discretization (Hara *et al.* 2008).

2.1 Experimental procedure

The R/C shell has the cylindrical shape with 950 mm × 950 mm square plan and has 688.75 mm radius and 10 mm thickness. ϕ0.75 mm stainless steel wires are used as the reinforcements and are placed in the middle of the shell thickness in both meridional and hoop direction with equi-distance 5 mm (see Fig. 1). The specimen is made by using the steel molds with machinery finishing to

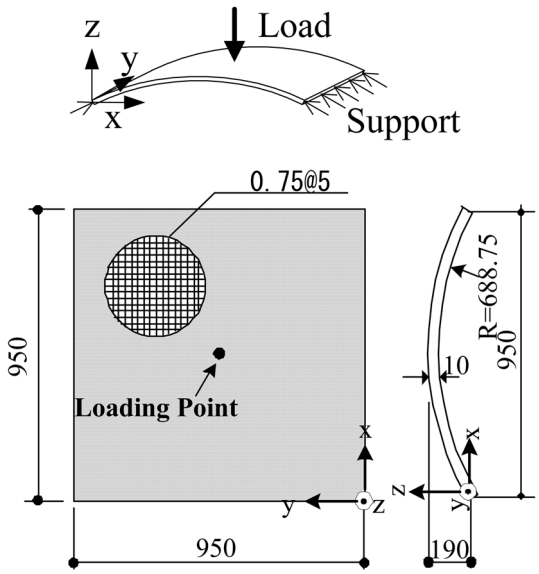

Fig. 1 Experimental model (Unit:mm)

Table 1 Material properties of concrete

Compressive strength (MPa)	41.4
Tensile strength(MPa)	4.10
Young's modulus(GPa)	26.7
Poisson's ratio	0.27

Table 2 Material properties of steel

Yield stress (MPa)	449
Tensile stress (MPa)	521
Young's modulus (GPa)	200
Tangential modulus (GPa)	20

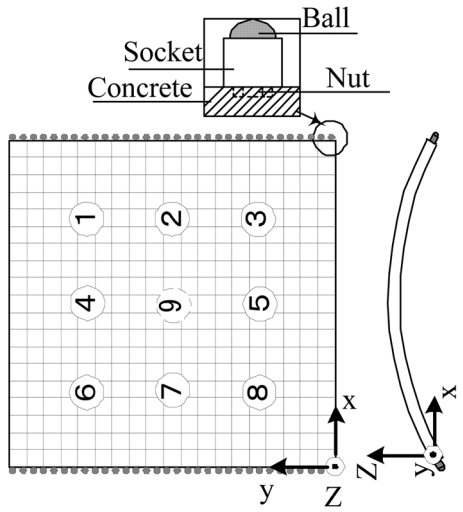

Fig. 2 Supporting condition and measuring points

minimize the initial geometric imperfections. In experiments, the micro concrete with aggregate size 2.5 mm is used. The material properties are shown in Table 1 and 2.

Experimental works are done by monotonic loading under the displacement increment controlled by a servo actuator oil jack system. Concentrated load is applied at the center of the specimen as shown in Fig. 1. Specimens are pin supported longitudinally on meridional edges by steel ball-hinge of 11 mm diameter arranged at 20 mm spaces to represent the same boundary conditions as the numerical one (see Fig. 2). Concentrated load is applied monotonically and the displacements are measured by displacement transducers placed at the measuring points (see circled numbers in Fig. 2) at every loading step.

2.2 Numerical procedure

The finite element method is adopted for the nonlinear analysis of the R/C shell. The detail procedure is given in previous papers (Hara *et al.* 1996, 2003). An isoparametric degenerated shell element is selected to model a numerical problem. Also, the R/C shell is divided into layered elements to represent the stresses distributions through the shell thickness. The Green Lagrange nonlinear strain definitions are adopted. To represent the concrete behavior, the following assumptions are adopted.

1. The Drucker Prager criterion is defined for the biaxial stress states (Hinton *et al.* 1984)

$$f(I_1, J_2) = \sqrt{\beta(3J_2) + \alpha I_1} = \sigma_0 \tag{1}$$

where I_1 and J_2 are the mean normal stress and the shear stress invariant, respectively. α and β are constants obtained from experimental results. In this paper, α and β are taken as 0.355 σ_0 and 1.355, respectively, based on the Kupfer's experiment (1969) and σ_0 is the equivalent stress.

To define the strain hardening rule, the relationship between the accumulated plastic strain and the equivalent stress is assumed to be the conventional 'Madrid Parabola' (Fig. 3) and is represented as follows:

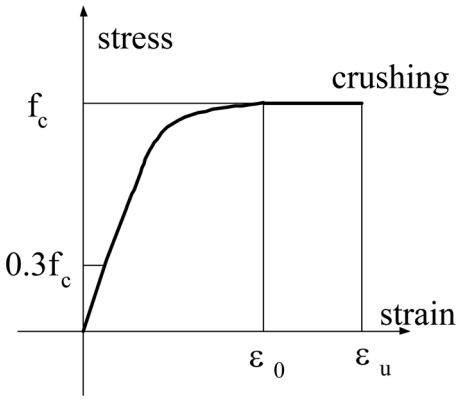

Fig. 3 Madrid Parabola

$$\sigma = E_0\varepsilon - \frac{1}{2}\frac{E_0}{\varepsilon_0}\varepsilon^2 \tag{2}$$

where E_0 and ε_0 represent the initial elastic modulus and the total strain at peak stress, respectively. It is assumed that the initial yield begins when the equivalent stress exceeds $0.3f_c$ (f_c: compressive strength of concrete). The crushing condition of concrete is described as a strain control phenomenon and the crushing condition is defined as akin to the yield condition representing in Eq. (1).

2. For concrete in tension, tension stiffening is introduced (Hara *et al*. 1996). In this model, the concrete behaves as the linear elastic material up to the tensile strength and after the peak stress, the stress is assumed to degrade linearly.

The reinforcing steel has a uniaxial bilinear constitutive relation in both compression and tension.

For the numerical analysis, a quarter of the whole structure is adopted because of the symmetry of supporting and loading conditions. The model is divided into 121 elements (11 divisions in both hoop and meridional directions) and each element is divided into 8 concrete layers and 2 steel layers. Boundary conditions are pin supported along meridional ends and are free along hoop ends to represent the same boundary condition as the experiments. In the numerical analysis, the geometric and material nonlinearlities are considered. The 9 node Heterosis element is used and 2×2 selective integration is adopted. The numerical simulation is performed under the displacement increment scheme. The yield condition of concrete is defined as the Drucker-Prager type (see Eq. (1)). The crushing condition is controlled by strain. The ultimate compressive strain of concrete 0.003 is adopted as in Kupfer's experiment (Kupfer 1969). Also, after cracking of concrete, the tension stiffening parameters accounting for the tension strength of concrete are introduced. The material nonlinearlities of steel is bilinear stress-strain relation for the reinforcement.

2.3 Numerical and experimental results

Fig. 4 shows the load-displacement relation obtained from experiments at ④⑥⑦⑨ shown in Fig. 2. Fig. 5 shows the load-displacement relation obtained from numerical analysis at the same points. The displacements along with the central meridian ④ and ⑨ represent downward and the displacement

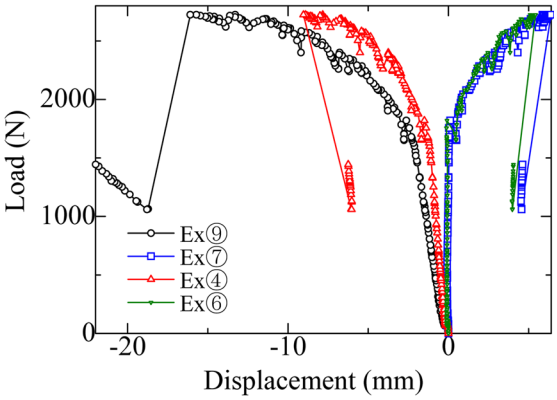

Fig. 4 Load-displacement relation (Experiment)

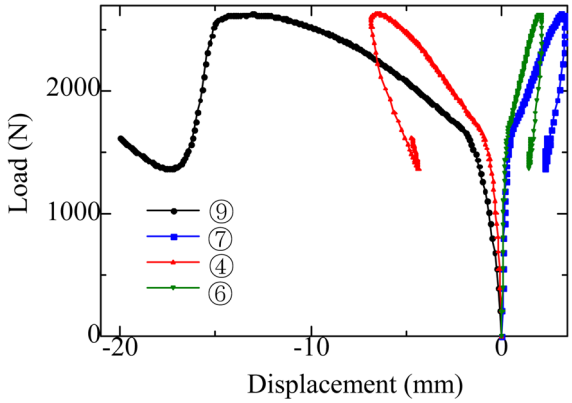

Fig. 5 Load-displacement relation(Numerical)

along with the outer meridian ⑥ and ⑦ shows upward. Therefore, the R/C shell deforms as akin to an arch structure.

From load-displacement relationship, both experimental and numerical results show the same tendencies and represent the failure when the maximum displacement reaches about 15 mm at the center point (see Fig. 6).

3. Compressive strength of R/C columns

Concrete columns are often used for the building frame system and the bridge piers to resist against the axial compression. The high strength concrete brings us the high compressive strength material. However, the tensile strength of this concrete is small even with increasing the compressive strength. In this chapter, the behavior of high strength concrete column is simulated by the finite element method The concrete column is represented as the solid elements. The material

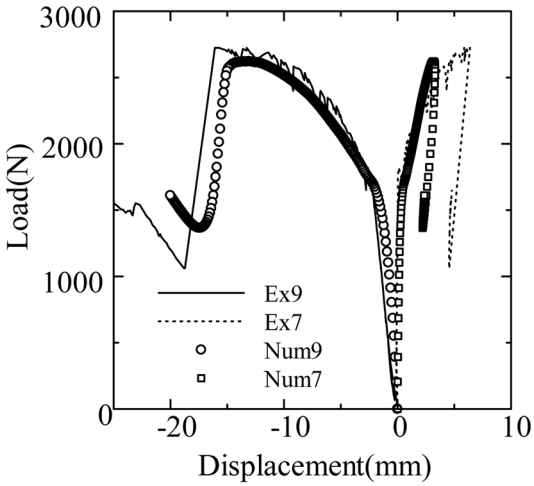

Fig. 6 Comparisons between numerical (Num) and experimental (Ex) results

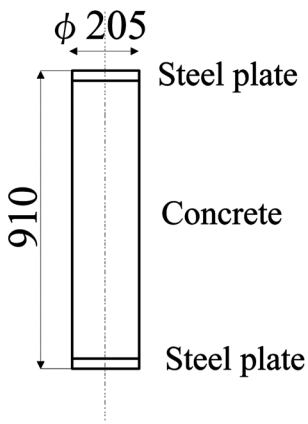

Fig. 7 Column model (unit:mm)

constants are determined from the experimental data (Hara *et al*. 2005). They are used for the numerical analyses.

3.1 Concrete column

Fig. 7 shows the dimensions of the specimen. The length of the columns is 910 mm. The column is cylindrical in shape and the diameter is 205 mm. The axial load is applied to the end plates of the column. Column is made by plane concrete and no reinforcements in the column and the steel end plate is placed at both ends of concrete column. The steel plate and the concrete are connected each other.

3.2 Numerical procedure

In numerical analyses, the finite element procedure is adopted (Hinton *et al.* 1986). The isoparametric hexahedral element with 20 nodes is adopted in the analysis. Concrete column is divided into such three dimensional elements because of taking Poisson's effects of compressed concrete into consideration.

The inelastic behavior of concrete possesses the recoverable strain components and irrecoverable strain components. Under tri-axial stress state, the yield function depends not only on the mean normal stress I_1 but also on the second deviatoric stress invariant J_2 (see Fig. 8). The yield condition of triaxial compressive concrete is expressed as Eq. (1).

The crushing condition of concrete is described as a strain control phenomenon and is defined as like as the yield condition in Eq. (1).

The response of concrete in tension is modeled as a linear-elastic brittle material and maximum tensile stress criteria are employed. To represent the tension cut off of the concrete in the tensile zone, three-dimensional stress relations in tension-compression status are considered (see Fig. 9). To represent the stiffening of reinforced concrete after cracking, the stress reduction of the concrete normal to the cracked plane is assumed as shown in Fig. 10. The stress in degradation zone is defined as follows.

$$\sigma = f_t' \exp\left(-\frac{\varepsilon - \varepsilon t'}{\gamma}\right) \qquad \gamma = \frac{G_f - 0.5 f_t' \varepsilon_{cr} l_c}{f_t l_c} \tag{3}$$

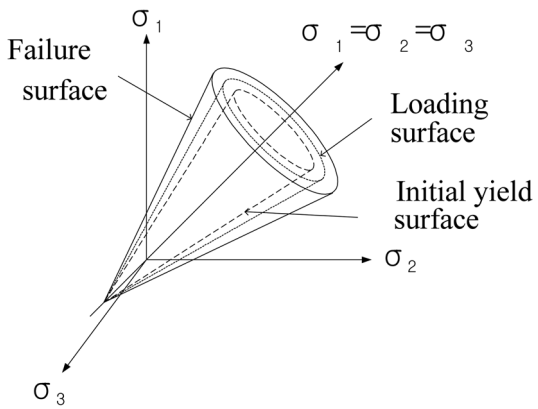

Fig. 8 Stresses in compression

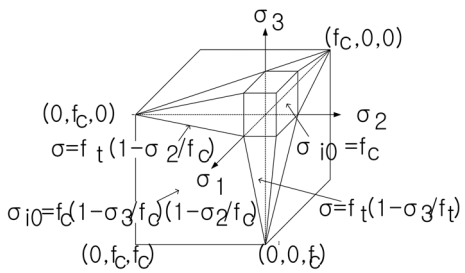

Fig. 9 Crack condition

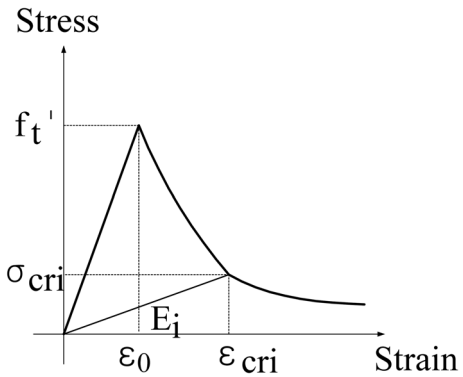

Fig.10 Stress strain in tension

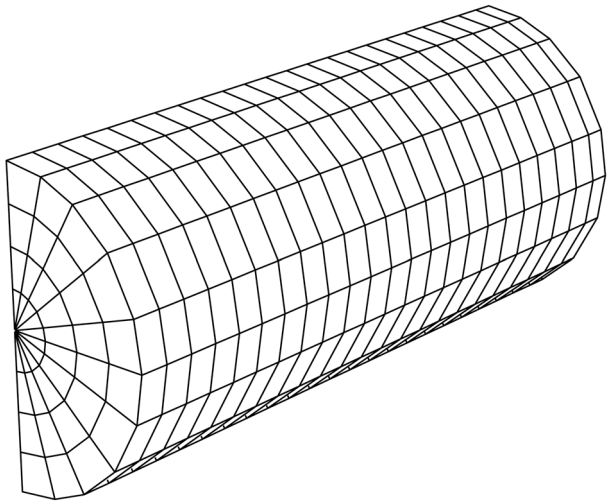

Fig. 11 FE model

where f_t' is the maximum tensile strength of concrete, γ the tension stiffing parameter, ε_t' the cracking strain, G_f the fracture energy of concrete, l_c the cubic root of volume in Gaussian point and ε_{cr} the strain in crack. $\gamma = 0.2$ is adopted herein. When the strain reversal appears the relation between the stress and the strain is defined using the modulus E_i.

3.3 Numerical model

To solve concentrically loaded column, the column is modelled as shown in Fig. 11. The numerical model of a column is a quarter of the whole structure because of the symmetry of the supporting and loading condition. A quarter of the model is divided into 920 elements and 4841 nodes. The applied load is defined as a uniformly distributed load under a concentric loading. In numerical analysis, the load is applied so as the nodal displacements on the end surface of the column show same value.

3.4 Numerical and experimental results

To represent the load deflection behaviour of the plain concrete column, the column without any reinforcement (plain concrete column) is analysed under the concentric load. Fig. 12 shows the relation between an axial load and column displacements. Circles and triangles show the lateral deflection at the column centre and the axial displacement at an end of the column. Fig. 12 shows the linear relationship up to 2000 kN of both displacements. Also, the lateral displacement at the centre of the column does not appear at this loading stage. After that, the lateral deformation grows rapidly and the column fails at 2295 kN. This phenomenon shows the sudden expansion of the concrete around the central portion of the column. As the compressive strength of the concrete is 73.6 MPa, concrete column could represent the strength of 2429 kN in compression test. Therefore, the column fails for its material strength.

Fig. 13 shows the failure pattern of the plain concrete column. From the figure, the global failure occurs at the centre of the cylinder. Due to the assumption of the simultaneous displacement on the end surface and the radial displacement constraint at both ends, R/C column fails shown in Fig. 13.

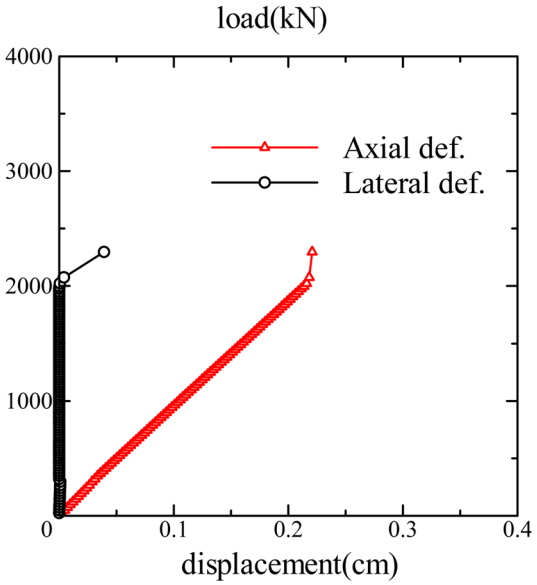

Fig. 12 Load deflection behavior of plain concrete column under concentric load

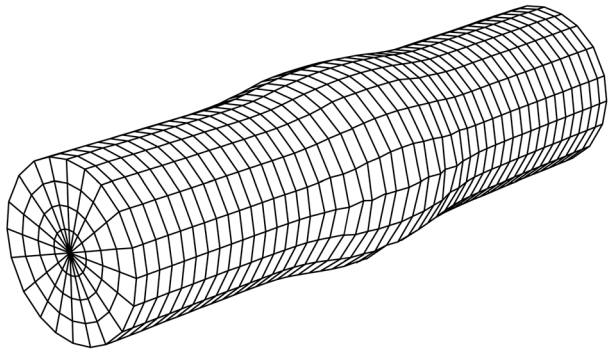

Fig. 13 Failure pattern of plain concrete column under concentric load

The numerical result shows the failure mechanisms appropriately.

4. R/C cooling tower response under seismic loading

Based on these results mentioned above, FEM procedures are applied to the huge R/C cooling tower structures. In this analysis, the parallel computing procedures are introduced into these analyses to reduce the computational efforts. R/C cooling tower has huge R/C shell supported by discrete R/C columns. The dynamic performances of R/C cooling tower are also computed by the application of parallel computations for dynamic analyses as well.

4.1 Numerical model

Fig. 14 shows the numerical model of R/C cooling tower with V-columns. The geometric configuration of R/C shell is defined as follows (Eckstein *et al.* 1998)

$$r = \Delta r + a \cdot \sqrt{1 + \frac{(z-125)^2}{b^2}} \tag{4}$$

where r is the radius of the shell at height z(m). Parameters a, b and Δr are shown in Table 4. Also, the radius and the thickness of R/C shell are presented in Table 5.

Reinforcements are placed in both hoop and meridional directions on both inner and outer surface of the shell. The reinforcing ratio of each reinforcing layer is assumed to be 0.2%. The concrete covers are 15% thickness of the shell wall from both inner and outer surfaces. The material properties of the concrete and the reinforcements are shown in Table 6.

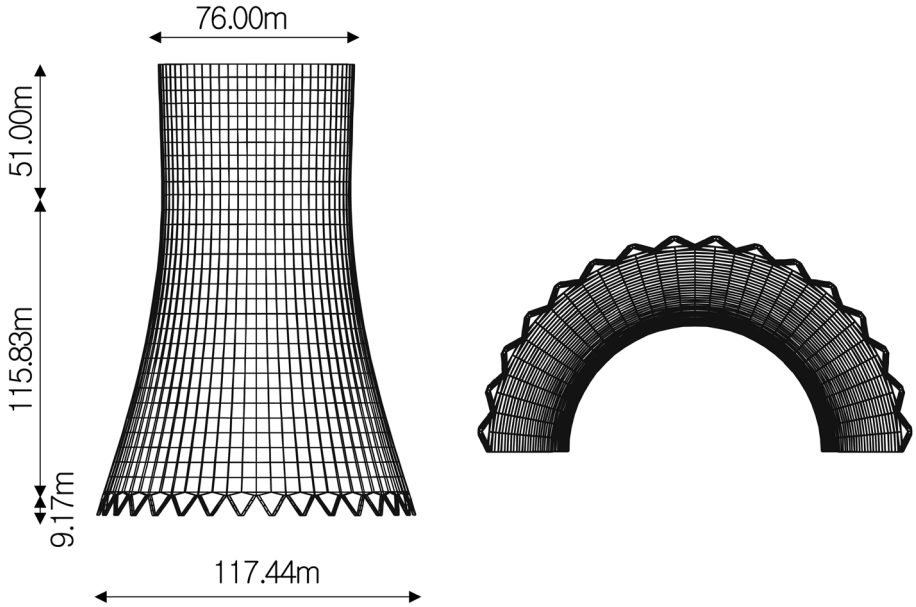

Fig. 14 Numerical models of cooling tower with V-columns

Table 3 Material properties of concrete

Compressive strength (MPa)	Tensile strength (MPa)	Young's modulus (GPa)
73.6	4	30

Table 4 Configuration parameters

Height(z)	*A*	*b*	Δr
9.17 m-125 m	51.9644	113.9896	-15.3644
125 m-176 m	0.2578	8.0293	36.3422

Table 5 Radius and thickness of the shell

	Lintel	Node	Top
Height(z)	9.17 m	125 m	176 m
Radius(m)	58.72 m	36.6 m	38.0 m
Thickness(m)	1.05 m	0.24 m	0.2 m

Table 6. Material properties

Concrete		Reinforcement	
Elastic modulus	34 GPa	Elastic modulus	206 GPa
Poisson's ratio	0.167	Tangent modulus	2.1 GPa
Density	0.0023 kg/cm^3	Yield stress	500 MPa
Compressive strength	36 MPa		
Tensile strength	2.7 MPa		

The model is divided into 32 elements in hoop direction and into 30 elements in meridional direction. A half of the R/C shell is adopted. Numerical model has 32 columns placed with equidistance along the lintel. Each column has 90 cm square cross sections and is divided into 4 elements with solid model represented in the previous chapter along the column height. Reinforcements are placed 2% in the columns. Numerical procedures are also the same as the previous chapter

4.2 Parallel procedure

For each element, the element stiffness **k** and the element mass matrices **m** are defined under the assumption mentioned above. Assembling these matrices the dynamic equilibrium equations are derived. During the time increment, the dynamic equilibrium equation is represented as follows

$$\mathbf{M}\Delta\ddot{\mathbf{y}}+\mathbf{C}\Delta\dot{\mathbf{y}}+\mathbf{K}\Delta\mathbf{y}=-\mathbf{M}\mathbf{I}\Delta\ddot{\mathbf{y}}_0 \tag{5}$$

where $\mathbf{M}$ is the mass matrix, $\mathbf{C}$ is the damping matrix, $\mathbf{K}$ is the stiffness matrix, $\Delta\mathbf{y}$, $\Delta\dot{\mathbf{y}}$, $\Delta\ddot{\mathbf{y}}$ are the response displacement, the response velocity and the response acceleration vector, respectively. $\Delta\ddot{\mathbf{y}}_0$ is the ground acceleration motion and Δ denotes the incremente. In this analysis, Raileigh damping is adopted to define the damping matrix.

In the dynamic response of structure, Eq. (5) is solved step by step. Applying the Newmark β method to Eq. (5), following equivalent stiffness equation is obtained.

$$\tilde{\mathbf{K}}\mathbf{y}=\tilde{\mathbf{f}} \tag{6}$$

where

$$\tilde{\mathbf{K}}=\frac{\mathbf{M}}{\beta\Delta t^2}+\frac{\mathbf{C}}{2\beta\Delta t}+\mathbf{K}$$

$$\tilde{\mathbf{f}}=-\mathbf{M}\mathbf{I}\Delta\ddot{\mathbf{y}}_0+\mathbf{M}\left(\frac{\Delta\dot{\mathbf{y}}}{\beta\Delta t}+\frac{\Delta\ddot{\mathbf{y}}}{2\beta}\right)+\mathbf{C}\left\{\frac{\Delta\dot{\mathbf{y}}}{2\beta}+\left(\frac{1}{4\beta}-1\right)\Delta\ddot{\mathbf{y}}\Delta\mathbf{t}\right\} \tag{7}$$

However, to solve this equation, a large computing effort is required. To overcome these problem, element-by-element (EBE) solution technique (Hara 2004, 2007) based on a parallel computation (Adeli *et al.* 1999) is applied to Eq. (6). In applying the preconditioned conjugate gradient solution techniques to Eq. (6), it will be solved by use of EBE. PC cluster is applied to solve the cooling tower with columns. PC cluster is composed of 8 personal computers and a switching hub to connect each other. The data communication of each computer is governed by MPI.

In the conjugate gradient scheme, the solution vector $\mathbf{y}_{k+1}$ and the gradient vector $\mathbf{r}_{k+1}$ are represented as follows

$$\mathbf{y}_{k+1}=\mathbf{y}_k-\alpha_k\mathbf{P}_k \tag{8}$$

$$\mathbf{r}_{k+1}=\mathbf{r}_k-\alpha_k\tilde{\mathbf{K}}\mathbf{p}_k \tag{9}$$

where

$$\alpha_k=\frac{\mathbf{r}_k^T\mathbf{r}_k}{\mathbf{p}_k^T\tilde{\mathbf{K}}\mathbf{p}_k} \tag{10}$$

and

$$\mathbf{p}_{k+1} = \mathbf{r}_k + \beta_{k+1}\mathbf{p}_k \tag{11}$$

$$\beta_{k+1} = \frac{\mathbf{r}_{k+1}^T \mathbf{r}_{k+1}}{\mathbf{r}_k^T \mathbf{r}_k} \tag{12}$$

In Eq. (8) through Eq. (12), $\tilde{\mathbf{K}}\mathbf{p}_k$ is calculated element by element. Therefore, these are easy to parallelized. To define the vector $\mathbf{r}_0$, the preconditioning technique is usually adopted. In this analysis, the solutions are relatively stable and the iterative solution converges well. Therefore, the preconditioning of the equation is not adopted to solving Eq. (6) by the conjugate gradient scheme.

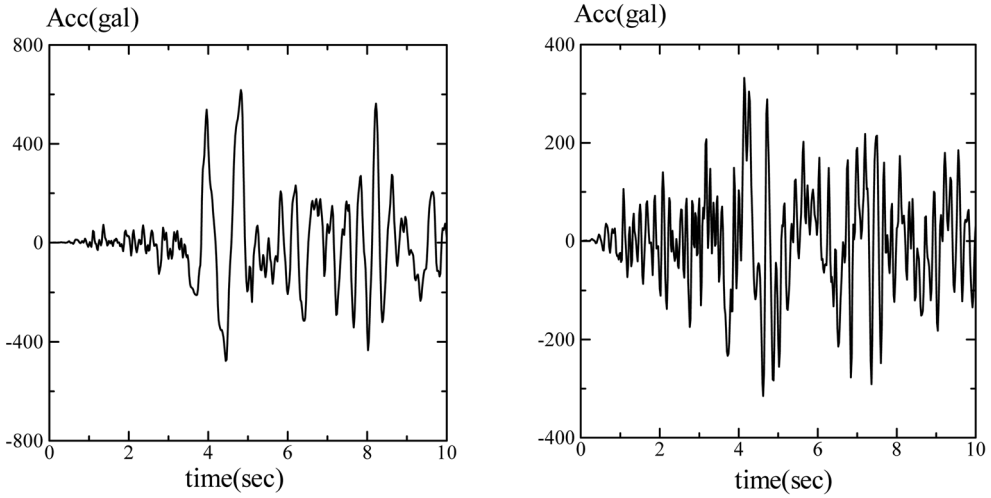

(a) NS component (b) UD acceleration

Fig. 15 Earthquake records in Kobe 1995

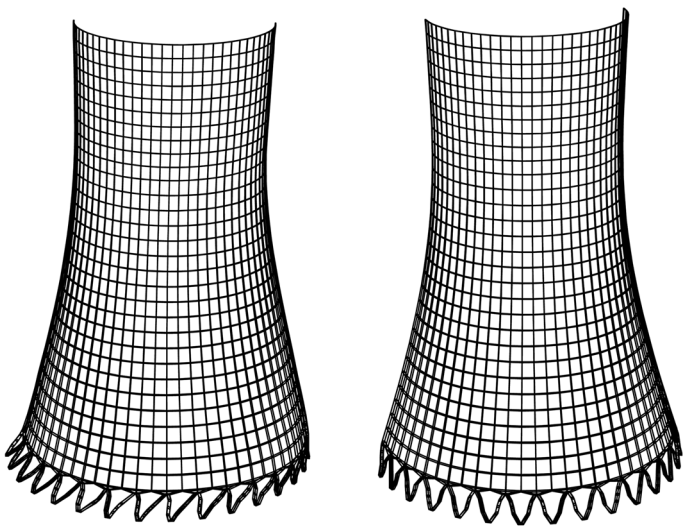

(a) NS (b) UD

Fig. 16 Deformations under Kobe 1995

4.3 Numerical results

In numerical analyses, after the gravity load is applied, seismic loads are induced into R/C cooling tower according to the NS and UD records shown in Fig. 15. In numerical analysis, the damping effects are not considered.

Fig. 16 shows the deformation pattern of the cooling tower under the same loading conditions, respectively. The response histories are as follows: The columns respond small deformation with R/C shell under initial earthquake loading. However, the columns start local deformation and initiate cracking at both ends under small loading (72gal in NS and 105gal in UD). Cracks propagate due to

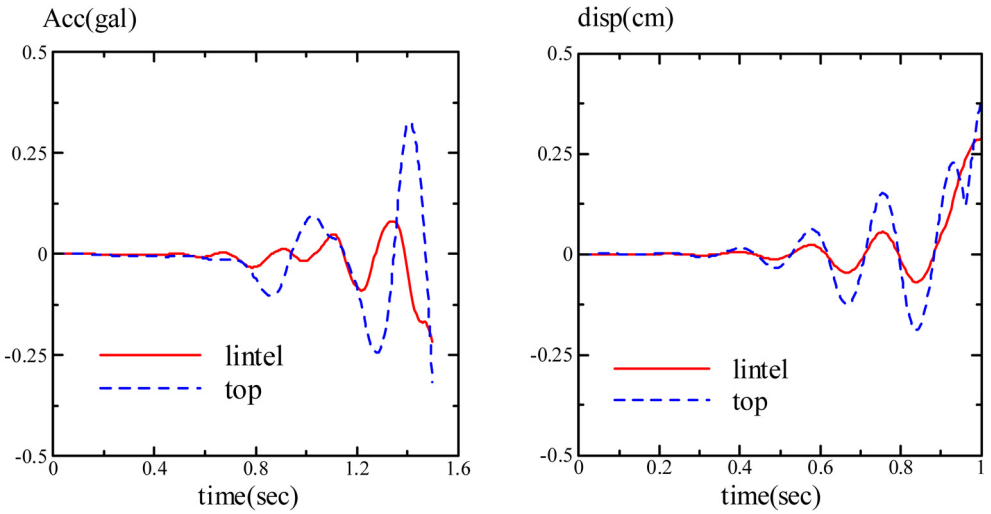

Fig. 17 Cooling tower under seismic load

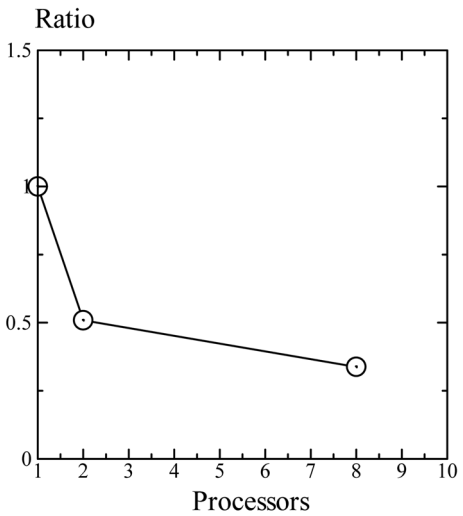

Fig. 18 Computing time and processors

the stress redistribution and additional applied loading. Then, the columns lose their rigidities and fails. Cracks arise due to flexure and shear at both ends of the columns. From the response analysis, the rigidity of the supporting columns is quite important factor for cooling tower to resist the seismic loading.

Fig. 17 shows the dynamic response of cooling tower at lintel and at the top under NS and UD earthquake acceleration record components, respectively. In both cases, the response shows the nonlinearity by the column cracking. The lintel response shows strong nonlinearity under lateral (NS) acceleration. On the other hand, both the lintel and the shell top responses show strong nonlinearity under vertical (UD) acceleration.

Fig. 18 shows the relation between computing time and the number of the processors. The loading condition is the step load of amplitude 0.01 g and the duration is 1.0 sec with time step $\Delta t = 0.0001$ sec. The ordinate shows the ratio of the computing time for each computing node to that for the one computing node. From the numerical results, the parallel computing reduces the computational time efficiently. In this analysis, the computing time of 8 processors shows three times of single processor without any particular programming optimization. In the EBE procedure, the computing memory storage is also reduced.

5. Conclusions

In this paper, FE computational technologies are applied to solve R/C shell structures. The static responses of both R/C shell structure and R/C columns are analyzed numerically and experimentally. Then the dynamic response of huge R/C structure is solved by use of FE procedure. From the numerical results, following conclusions are obtained.

1. Degenerate shell elements are applicable to analyze R/C thin shell structure and the numerical results well simulate the experimental analyses.
2. Solid elements are also applicable to analyze the solid bodies such as columns and beams. In the case of the model with large numbers of unknowns due to model the structure by the solid element, EBE parallel procedures are also applicable.
3. EBE parallel FE procedures are applicable to solve the R/C huge structure with small deviations under dynamic excitation. Therefore, parallel computing is also efficient for solving dynamic problems of concrete structures.
4. Consequently, from the numerical analyses, it is concluded that the conventional FEM procedures combined with computational technologies are enable us to design the huge R/C structures with small deviations statically and dynamically. The numerical scheme is applicable to the practical one such as the earthquake response of the structure or the response of the dynamic wind loading considering the structural performances.

References

Adeli, H. and Soegiarso, R. (1999), *High-performance computing in structural engineering*, CRC Press.

Busch, D., Harte, R., Krätzig, W.B. and Montag, U. (2002), "New natural draft cooling tower of 200 m of height", *Eng. Struct.*, **24**, 1509-1522.

Eckstein, U. and Nunier, F.J. (1998), "Specific design and construction details of the Boxberg cooling tower",

Eng. Struct., **20**, 862-867.
Hara, T., Kato, S. and Gould, P.L. (1996), "Ultimate strength of R/C cooling tower shells with various reinforcing ratio", *J. IASS,* **37**(3), 153-163.
Hara, T., Shigematsu, T. and Tamura, T. (2003), "Behavior of R/C cylindrical shell under lateral load", *Struct. Eng. Mech.*, **16**(3), 361-369.
Hara, T. (2004), "Dynamic response analysis of R/C cooling tower shell", *WCCM VI in conjunction with APCOM'04,* Beijing, China.
Hara, T. and Hadi, M.N.S. (2005), "Behavior of high strength concrete columns under eccentric loading", *Proceedings of the Tenth International Conference on Civil, Structural and Environmental Engineering Computing,* 16.
Hara, T. (2007), "Dynamic response of cooling tower shell under seismic loading", *Struct. Eng. World Congress.*
Hara, T. (2008), "Numerical and experimental evaluation of R/C shell", *Proceedings of International Conference on Advances in Struct. Eng. Mech.,* 133-144.
Harte, R. and Wittek, U. (2009), "Recent development of cooling tower design", *50th Anniversary Symposium of the International Association for Shell and Spatial Structures Valencia* (on CDROM).
Hinton, E. and Owen, D.J.R. (1984), *Finite element software for plates and shells*, Prineridge Press, Swansea, UK.
Hinton, E. and Owen, D.R.J. (1986), *Numerical methods and software for dynamic analysis of plates and shells*, Pineridge Press, Swansea, U.K.
Kupfer, H. and Hilsdorf, K.H. (1969), "Behavior of concrete under biaxial stress", *ACI J.,* **66**(8), 656-666.
Levit, I. (1987), "Element-by-element solvers of order N", *Comput. Struct.* **27**, 357-360.